

Common-Mode Frequency of Power Systems Affected by Voltage Dynamics

Huisheng Gao, Huanhai Xin, Guang Hu, Bin Cao, Hui Yuan, and Linbin Huang

Abstract—The high penetration of converter-interfaced generation (CIGs) in power systems has raised concerns regarding the risk of frequency collapse. However, most existing theoretical analysis methods for system frequency assume constant bus voltages, which can lead to inaccurate results and potentially incorrect conclusions. The main challenge lies in the absence of analytical models that consider voltage dynamics when representing the system-level frequency. To address this issue, this article defines the voltage-influenced common-mode frequency (VCMF), which captures the dynamics of the system frequency in the scenario of non-constant bus voltages. The derivation process is implicitly based on the strong relationship between the consistent part of the bus frequencies (i.e., system frequency) and the rotational invariance of power flow. The expression of VCMF demonstrates that non-constant voltages affect the system frequency through a global term that involves the dynamics of all the devices, making its analysis challenging. Therefore, a network partitioning method based on the algebraic graph theory is proposed, which effectively divides the globally coupling term into several locally coupling terms, enabling a more tractable analysis of VCMF. Finally, simulations are used to validate the proposed method and confirm its validity.

Index Terms—Frequency stability, voltage-influenced common-mode frequency (VCMF), system frequency representation, voltage dynamics, network partitioning.

I. INTRODUCTION

POWER systems are experiencing rapid development due to the widespread implementation of renewable energies that are connected to power grids via power electronic converters. The low inertia and weak frequency regulation capability of converter-interfaced generations (CIGs) pose great challenges to the frequency stability of power systems [1]. Notably, recent blackouts in England and Texas have demonstrated the vulnerability of system frequency, leading to substantial frequency deviations and necessitating widespread load shedding [2]–[3]. Consequently, it becomes imperative to conduct a comprehensive analysis of the frequency responses of modern power systems to support the rapid development of renewable energy sources.

Frequency stability analysis, according to some widely accepted definitions [4]–[5], focuses on the system frequency, which represents the consistent part of the frequency response at each bus and reflects the overall frequency behavior of the power system. Currently, there are mainly two approaches for analyzing the system frequency: time-domain simulation and analytical modeling [6]. The former provides more accurate results by considering the detailed dynamics of the system.

However, it lacks a mechanism explanation, which makes it challenging to provide theoretical insights for enhancing frequency stability. Moreover, conducting simulations to verify frequency stability under various conditions can be computationally intensive. In contrast, the analytical model-based analysis offers theoretical foundations and relatively lower computational complexity, making it widely applicable.

To develop an analytical model of the system frequency, it is important to reflect the concept of system frequency, as the actual frequency response of power systems has spatial distribution differences, especially when a large number of CIGs are integrated. Currently, the frequency of the center of inertia (COI) is widely acknowledged as the system frequency [7]. Building upon this concept, researchers have developed various classic analytical models of system frequency, including the average system frequency (ASF) [8] and system frequency response (SFR) [9]. Many of the latest models are derived from these existing concepts.

However, traditional methods based on COI and ASF/SFR may not be suitable for rigorously and accurately analyzing the frequency characteristics of modern power systems, due to their theoretical limitations. For instance, the calculation of COI frequency relies on devices' inertia, and it may not be feasible to apply COI frequency in low-inertia systems, (e.g., all generators are droop-based converters). Additionally, the ASF and SFR assume constant bus voltages and only analyze the relationship between the frequency and active power (F-P) of devices, which may lead to inaccurate analysis [10]. For example, a case study in [11] demonstrated that assuming constant voltage can result in an error of approximately 30% when evaluating the frequency nadir under a disturbance.

Based on the above discussions, it is clear that there is still ambiguity regarding the concept of the system frequency and how to analytically represent it. Our previous work has made a step forward by obtaining the common-mode frequency (CMF) component through frequency response decoupling under the assumption of constant voltages. We show that CMF can represent system frequency better than the COI frequency and ASF, which demonstrates that system frequency may be a frequency component rather than an inertia-weighted average of bus frequencies [12]. However, the CMF approach relied on the assumption of constant voltages and could not explain the impact of voltage dynamics on the system frequency.

To address the aforementioned issues, this paper defines the voltage-influenced common-mode frequency (VCMF) to represent the system frequency in the scenario of non-constant voltages, which is an extension of CMF. The VCMF is obtained from the decomposition of system closed-loop transfer function matrix. It provides a comprehensive analysis of the system frequency by considering both the direct F-P

response of devices (such as inertia), and the indirect F-P response induced by voltage dynamics, whose action path is “F-Q-V-P”. We demonstrate it by a system involving a converter equipped with F-Q droop (as proposed in [13]) and a nearby constant impedance load (CIL). When the frequency (F) drops, the reactive power (Q) output by the converter decreases, causing a decrease in load voltage (V) and active power (P) consumption, which consequently facilitates the recovery of frequency. By incorporating the indirect F-P response, the VCMF is much more accurate than traditional ASF and previous CMF.

In addition, the indirect F-P response exhibits globally coupling characteristics as it involves all devices and the transmission network in the system. To deal with this, a network partitioning method based on the algebraic graph theory is introduced, which identifies and cuts off weak paths in the indirect F-P response, effectively transforming it from a globally coupling term into several locally coupling terms. Then an approximate VCMF model is obtained, which is much easier to analyze.

The main contributions of this work are as follows:

1) The VCMF is defined by decomposing the bus frequencies in the scenario of non-constant voltages. It shows that the essence of the consistency of bus frequencies results from the rotational invariance of the power flow, which provides a new perspective for understanding the system frequency response. Notably, the VCMF can represent the system frequency in the case of zero inertia, where traditional COI frequency cannot be computed.

2) The VCMF analytically describes how voltage dynamics affect the system frequency, leading to significantly improved accuracy in frequency analysis compared to traditional methods like ASF. For example, the VCMF illustrates that the combination of F-Q droop control and nearby CILs is equivalent to F-P droop. This relationship, however, cannot be revealed using ASF.

3) The proposed network partitioning method utilizes the algebraic connectivity to assess the strength of the devices’ coupling, thus it effectively decomposes the globally coupled indirect F-P responses into several locally coupled terms, which facilitates the calculation and understanding of how voltage affects the system frequency, especially in large-scale power systems.

The rest of this paper is organized as follows: In Section II, the modeling of modern power systems is presented, and some general properties of the systems are introduced for the subsequent derivation. Section III defines the VCMF by decomposing the frequency response, then it is compared with several existing methods. Section IV proposes a network partitioning method using algebraic graph theory. In Section V, the proposed VCMF and network partitioning method are verified through numerical simulations. Finally, conclusions are drawn in Section VI.

Notation: We denote by $\mathbf{0}$ and $\mathbf{1}$ the column vectors or matrices with appropriate dimensions, whose elements are respectively all 0 and 1. We use ω_0 to denote the nominal frequency in rad/s. Given a vector $\mathbf{x} = [x_1, \dots, x_n]^T$ or a set of variables x_i , $\text{diag}\{\mathbf{x}\}$ or $\text{diag}\{x_i\}$ denotes the diagonal matrix whose i -th diagonal element is x_i . We use $\text{triu}(\mathbf{A})$ to denote the

upper triangular matrix of \mathbf{A} . We use “ s ” to denote the Laplace variable, and “ \mathbf{s} ” to denote the diagonal matrix $\text{diag}\{\mathbf{s}\}$ with appropriate dimensions. For notational simplicity, “ s ” is omitted if not confusing the understanding.

II. MODELING OF POWER SYSTEMS FOR SYSTEM FREQUENCY ANALYSIS WITH NON-CONSTANT VOLTAGE

This section presents power system models that are suitable for analyzing the system frequency under non-constant voltage scenarios. In addition, some properties of the generation devices and the transmission network are introduced, which will be utilized in the derivation and simplification of VCMF in Sections III and IV, respectively.

A. Modeling of Power Systems

Generally, power systems can be conceptualized as multi-input multi-output feedback control systems [14], as depicted in Fig. 1, which can be divided into two parts: generation devices (such as SGs and CIGs) and transmission network. In the following, we will model these two parts separately.

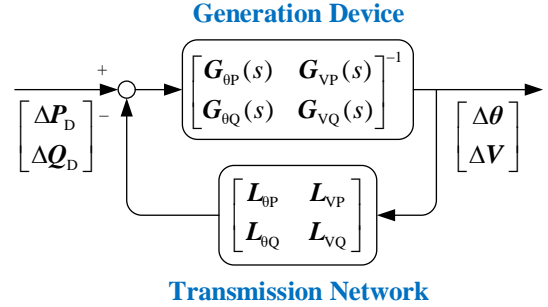


Fig. 1. Closed-loop model for system frequency analysis.

1) *Generation Devices:* The generation devices can be represented by Jacobian transfer function matrixes, where the input is the phase angle/voltage amplitude, and the output is the active/reactive power:

$$\begin{bmatrix} \Delta \mathbf{P} \\ \Delta \mathbf{Q} \end{bmatrix} = - \begin{bmatrix} \mathbf{G}_{\theta P}(s) & \mathbf{G}_{VP}(s) \\ \mathbf{G}_{\theta Q}(s) & \mathbf{G}_{VQ}(s) \end{bmatrix} \begin{bmatrix} \Delta \boldsymbol{\theta} \\ \Delta \mathbf{V} \end{bmatrix} \quad (1)$$

where Δ denotes the perturbed value of a variable. The vectors $\Delta \mathbf{P}$ and $\Delta \mathbf{Q}$ (composed of ΔP_i and ΔQ_i , respectively) represent the active and reactive power outputs of generation devices, where i ranges from 1 to n , with n being the total number of generation devices. Similarly, the vectors $\Delta \boldsymbol{\theta}$ and $\Delta \mathbf{V}$ (composed of $\Delta \theta_i$ and ΔV_i , respectively) represent phase angles and amplitudes of the device internal voltages, where $\Delta \boldsymbol{\theta} = \omega s^{-1} \Delta \boldsymbol{\omega}$, $\Delta \boldsymbol{\omega}$ is the frequency vector composed of $\Delta \omega_i$. The transfer function matrix $\mathbf{G}_{\bullet}(s) = \text{diag}\{\mathbf{G}_{\bullet,i}(s)\}$ describes the dynamics of devices, where the subscript $\bullet \in \{\theta P, VP, \theta Q, VQ\}$ denotes the input and output. The negative sign before the transfer function matrix is due to the fact that devices provide positive active and reactive power responses when there is a frequency and voltage drop.

Three types of devices are considered: SGs, grid-following (GFL) converters and grid-forming (GFM) converters [15]. While they have distinct physical characteristics and control schemes, the analysis in this paper is generic and does not

> REPLACE THIS LINE WITH YOUR MANUSCRIPT ID NUMBER (DOUBLE-CLICK HERE TO EDIT) <

depend on these specific characteristics. Therefore, the specific models and Jacobian matrices of the devices are not presented in the main text, for the sake of clarity and readability, but are instead provided in Appendix.

It is worth noting that loads can be viewed as some special devices. Of particular interest, CILs can be interpreted as either devices or components of the transmission network. We will briefly discuss these two perspectives in the case study. But for the purpose of simplifying the analysis, CILs are predominantly treated as parts of the network, leading to a smaller number of devices.

2) *Transmission Network*: The transmission network is characterized by the power flow equations, which are adequate for the analysis of system frequency. The linearized power flow equations can be expressed as follows, similar models can be found in [14],[16]:

$$\begin{bmatrix} \Delta P \\ \Delta Q \end{bmatrix} = \begin{bmatrix} L_{0P} & L_{VP} \\ L_{0Q} & L_{VQ} \end{bmatrix} \begin{bmatrix} \Delta \theta \\ \Delta V \end{bmatrix} \quad (2)$$

where L_{\bullet} is the Jacobin matrix of the network. The explicit expressions of its (diagonal and off-diagonal) elements are

$$\begin{cases} L_{0P}[i, i] = V_{i0} \sum_{j \in \text{adj}(i)} V_{j0} (-G_{ij} \sin \theta_{ij0} + B_{ij} \cos \theta_{ij0}) \\ L_{0P}[i, j] = V_{i0} V_{j0} (G_{ij} \sin \theta_{ij0} - B_{ij} \cos \theta_{ij0}) \end{cases} \quad (3)$$

$$\begin{cases} L_{VP}[i, i] = \sum_{j \in \text{adj}(i)} V_{j0} (G_{ij} \cos \theta_{ij0} + B_{ij} \sin \theta_{ij0}) + 2V_{i0} G_{ii} \\ L_{VP}[i, j] = V_{i0} (G_{ij} \cos \theta_{ij0} + B_{ij} \sin \theta_{ij0}) \end{cases} \quad (4)$$

$$\begin{cases} L_{0Q}[i, i] = V_{i0} \sum_{j \in \text{adj}(i)} V_{j0} (G_{ij} \cos \theta_{ij0} + B_{ij} \sin \theta_{ij0}) \\ L_{0Q}[i, j] = V_{i0} V_{j0} (-G_{ij} \cos \theta_{ij0} - B_{ij} \sin \theta_{ij0}) \end{cases} \quad (5)$$

$$\begin{cases} L_{VQ}[i, i] = \sum_{j \in \text{adj}(i)} V_{j0} (G_{ij} \sin \theta_{ij0} - B_{ij} \cos \theta_{ij0}) - 2V_{i0} B_{ii} \\ L_{VQ}[i, j] = V_{i0} (-G_{ij} \sin \theta_{ij0} + B_{ij} \cos \theta_{ij0}) \end{cases} \quad (6)$$

where $j \in \text{adj}(i)$ means bus j ($j \neq i$) is adjacent to bus i ; G_{ij} and B_{ij} are respectively elements of the network admittance matrix $Y = G_B + jB_B$, θ_{ij0} is the steady angle difference between bus i and j , and V_{i0} is the steady voltage amplitude of bus i .

3) *Closed-loop System*: As illustrated in Fig. 1, by combing the devices and the network and applying power disturbance (ΔP_D and ΔQ_D), the closed-loop response of the system can be expressed as (7), where $H_{\bullet}(s) = G_{\bullet}(s) + L_{\bullet}$.

$$\begin{bmatrix} \Delta \theta \\ \Delta V \end{bmatrix} = \begin{bmatrix} H_{0P}(s) & H_{VP}(s) \\ H_{0Q}(s) & H_{VQ}(s) \end{bmatrix}^{-1} \begin{bmatrix} \Delta P_D \\ \Delta Q_D \end{bmatrix} \quad (7)$$

B. Some General Properties of the Devices and the Network

To facilitate the subsequent derivations in Section III and IV, some properties of the Jacobian matrix of the devices and the network are introduced here.

First, for devices, it is generally observed that $G_{0P}(s) \approx 0$ and $G_{0Q}(s) \approx 0$ in the low-frequency range. Additionally, devices with good voltage regulation capability, such as SGs and virtual synchronous generators (VSGs), can be effectively modeled as with a large $G_{VQ}(s)$. The reasons are as follows.

1) Regarding $G_{0P}(s)$, this transfer function of a generation device can be typically expressed as

$$G_{0P}(s) = \omega_0^{-1} (Js^2 + (K_{PFC}s + K_{SFC})G_D(s)) \quad (8)$$

where J is the inertia and K_{PFC} , K_{SFC} are the gains of primary and secondary frequency control (PFC/SFC), respectively; $G_D(s)$ represents the control delay and is approximately 1 in the low-frequency range. It is evident that $G_{0P}(s) \approx K_{SFC}/\omega_0$ when s is small. Generally, K_{SFC} is either zero or very small, and when divided by ω_0 (314 rad/s or 377 rad/s), it becomes even more negligible. Consequently, $G_{0P}(s)$ tends to be zero in the low-frequency range. 2) As for the $G_{0Q}(s)$, if it does not approach zero as s tends to zero, the reactive power output (and thus its voltage) will continue to increase in the quasi-steady state after frequency dips, similar to the behavior of SFC, which is undesired and devices are not designed to exhibit such behaviors. 3) A large $G_{VQ}(s)$ indicates that the device provides significant reactive support with a small voltage dip, enabling it to maintain a nearly constant voltage.

The next property to be introduced is the rotational invariance of power flow (with respect to phase angles) [18], which means that the power flow remains the same when the phase angles of all the buses are uniformly increased. Mathematically, it is manifested by the fact that both the network matrices L_{0P} and L_{0Q} have a right eigenvector of $\mathbf{1}$ with a corresponding eigenvalue of 0. In other words,

$$L_{0P}\mathbf{1} = 0, \quad L_{0Q}\mathbf{1} = 0 \quad (9)$$

This property serves as the foundation for the derivation of both the CMF presented in our previous work and the VCMF in the next section. Note that the coherency of bus phase angles corresponds to the coherency of bus frequencies.

Another important property to keep in mind is that large-scale power networks can typically be divided into multiple regions based on the electrical distance, where buses within each region are strongly interconnected while the coupling between regions is relatively weak [19]. Mathematically, this property is reflected in the approximate block diagonal dominance of network Jacobian matrices, indicating that the magnitudes of entries in the diagonal blocks are relatively larger than those outside the blocks. This property is useful when simplifying the calculation of VCMF, which will be discussed further in Section IV.

III. VOLTAGE-INFLUENCED COMMON-MODE FREQUENCY

This section defines VCMF by decoupling the bus frequencies to extract the common component. A comparison is then made among the VCMF and traditional COI frequency, ASF, and the previous CMF to showcase its superiority.

A. Derivation of VCMF

In our previous work, the CMF is derived by leveraging the rotational invariance of power flow. However, this method cannot be directly extended to systems with non-constant voltages since the invariance of power flow is only with respect to phase angles but not voltages. Consequently, it is impossible to decompose voltage responses alongside phase angle (or frequency) responses.

> REPLACE THIS LINE WITH YOUR MANUSCRIPT ID NUMBER (DOUBLE-CLICK HERE TO EDIT) <

To tackle this issue, it is crucial to recognize that the incorporation of voltage dynamics aims to achieve a more theoretically rigorous and accurate representation of the system frequency, rather than focusing on the analysis of voltage itself. Thus, voltage variables in (7) can be eliminated via a matrix transformation, as follows:

$$\Delta \mathbf{V} = -\mathbf{H}_{\text{VQ}}^{-1}(s) \mathbf{H}_{\text{0Q}}(s) \Delta \boldsymbol{\theta} + \mathbf{H}_{\text{VQ}}^{-1}(s) \Delta \mathbf{Q}_{\text{D}} \quad (10)$$

In addition, the frequency response to active and reactive power disturbances can be analyzed separately using the superposition principle. Since active power disturbance dominates frequency response, we will consider this disturbance as an example in the following. Substitute (10) and $\Delta \mathbf{Q}_{\text{D}} = \mathbf{0}$ into (7) yields

$$\Delta \boldsymbol{\theta} = \left(\mathbf{G}_{\text{0P}}(s) + \mathbf{L}_{\text{0P}} - \mathbf{H}_{\text{VP}}(s) \mathbf{H}_{\text{VQ}}^{-1}(s) \mathbf{H}_{\text{0Q}}(s) \right)^{-1} \Delta \mathbf{P}_{\text{D}} \quad (11)$$

$$:= \mathbf{R}^{-1}(s)$$

where $\mathbf{R}^{-1}(s)$ is the closed-loop transfer function between active power disturbance and phase angle response.

However, decomposing the phase angle in a strict manner remains challenging due to its lack of specific structural properties for decomposition. In this regard, we propose an approximate decomposition method by leveraging the properties of $\mathbf{R}^{-1}(s)$ (or $\mathbf{R}(s)$) in the low-frequency band. For the convenience of discussion, let $\lambda_k(s)$, $\mathbf{u}_k(s)$, $\mathbf{v}_k(s)$ ($k = 1, \dots, n$), respectively denote the k -th eigenvalue, right and left eigenvector of $\mathbf{R}(s)$, i.e.,

$$\mathbf{R}(s) = \sum_{k=1}^n \lambda_k(s) \mathbf{u}_k(s) \mathbf{v}_k^{\text{H}}(s) \quad (12)$$

Consider that $\mathbf{G}_{\text{0P}}(s) \approx \mathbf{0}$ and $\mathbf{G}_{\text{0Q}}(s) \approx \mathbf{0}$ when s is small (as discussed in Section II-B), then $\mathbf{R}(0)$ can be written as

$$\mathbf{R}(0) = \mathbf{L}_{\text{0P}} - (\mathbf{G}_{\text{VP}}(0) + \mathbf{L}_{\text{VP}}) (\mathbf{G}_{\text{VQ}}(0) + \mathbf{L}_{\text{VQ}})^{-1} \mathbf{L}_{\text{0Q}} \quad (13)$$

By combining (9) and (13), we can observe that $\mathbf{1}$ is a right eigenvector of $\mathbf{R}(0)$, with eigenvalue 0, i.e., $\lambda_1(0) = 0$, $\mathbf{u}_1(0) = \mathbf{1}$. For the convenience of discussion, we denote by \mathbf{c}/n (a column vector with elements c_i/n) the corresponding left eigenvector $\mathbf{v}_1(0)$, which satisfies $\mathbf{v}_1^{\text{T}}(0) \mathbf{u}_1(0) = 1$.

If we treat $\mathbf{R}(s)$ as the perturbation of $\mathbf{R}(0)$, then according to the matrix perturbation theory [20], $\lambda_1(s)$ can be approximately expressed as

$$\lambda_1(s) \approx \mathbf{v}_1^{\text{T}}(0) \mathbf{R}(s) \mathbf{u}_1(0) \quad (14)$$

By substituting (12) and (14) into (11), and assuming that $\mathbf{u}_1(s) \approx \mathbf{u}_1(0)$, $\mathbf{v}_1(s) \approx \mathbf{v}_1(0)$, then we can approximately obtain

one component of $\Delta \boldsymbol{\theta}$, whose differentiation is

$$\Delta \boldsymbol{\omega}_{\text{VCM}} = \frac{\mathbf{c}^{\text{T}} \Delta \mathbf{P}_{\text{D}}}{\sum c_i G_{\text{0P},i}(s) \underbrace{- \mathbf{c} \mathbf{H}_{\text{VP}}(s) \mathbf{H}_{\text{VQ}}^{-1}(s) \mathbf{H}_{\text{0Q}}(s) \mathbf{1}}_{\text{Voltage coupling term}}} \frac{s}{\omega_0} \mathbf{1} \quad (15)$$

This frequency component is consistent across all the buses, which is a typical characteristic of system frequency. Hence, it is defined as the “VCMF” in this paper. It can be inferred from the derivation that the consistency of bus frequencies is a result of the rotational invariance of power flow, rather than being attributed to inertia-weighted averaging.

It can be observed from (15) that the coefficient c_i in fact represents the weighting of each bus, similar to that in CMF. In addition, the VCMF involves both the direct F-P response (i.e., $G_{\text{0P},i}(s)$), as well as the indirect one, i.e., the second term in the denominator. It can be easily concluded by its subscripts that its action path is F-Q-V-P. Obviously, if $\Delta \mathbf{V} = \mathbf{0}$, this term is zero, indicating that this path arises from the voltage dynamics. Thus, it is referred to as the Voltage Coupling Term (VCT), and it will be further discussed in Section IV.

We note that the derivation is based on some approximations. For example, $\mathbf{u}_1(s) \approx \mathbf{u}_1(0)$, $\mathbf{v}_1(s) \approx \mathbf{v}_1(0)$, they are valid in the low-frequency range as discussed in Section II-B, where dynamics of the system frequency mainly belong to, which justifies the approximations.

B. Comparison of VCMF with Existing Analysis Methods

For a comprehensive understanding, the VCMF is compared with existing system frequency representation methods (COI frequency) and frequency analysis models (ASF). TABLE I summarizes the comparisons.

1) System Frequency Representation Methods

The COI frequency is the most widely accepted method for defining/representing system frequency. However, it lacks a rigorous theoretical foundation and is essentially heuristic. For example, it cannot account for the concept of system frequency in zero-inertia power systems that consist entirely of zero-inertia devices, such as droop-controlled converters.

Compared to COI frequency, CMF/VCMF is a frequency component obtained by decoupling based on the rotational invariance of power flow, which is less reliant on device characteristics such as inertia. Thus, they are more theoretically rigorous and more applicable (e.g., for zero-inertia systems).

TABLE I.
COMPARISON OF REPRESENTATIONS AND ANALYTICAL MODELS OF SYSTEM FREQUENCY

	COI	ASF	CMF	VCMF
Derivation	Average of bus frequencies	Average of bus frequencies	A frequency component	A frequency component
Expression	$\Delta \omega_{\text{COI}} = \frac{\mathbf{J}^{\text{T}}}{\mathbf{J}^{\text{T}} \mathbf{1}} \Delta \boldsymbol{\omega}^*$	$\Delta \omega_{\text{AS}} = \frac{s}{\omega_0} \frac{\mathbf{1}^{\text{T}} \Delta \mathbf{P}_{\text{D}}}{\sum G_{\text{0P},i}(s)}$	$\Delta \omega_{\text{CM}} = \frac{s}{\omega_0} \frac{\mathbf{c}^{\text{T}} \Delta \mathbf{P}_{\text{D}}}{\sum c_i G_{\text{0P},i}(s)}$	$\Delta \omega_{\text{VCM}} = \frac{s}{\omega_0} \frac{\mathbf{c}^{\text{T}} \Delta \mathbf{P}_{\text{D}}}{\sum c_i G_{\text{0P},i}(s) + \text{VCT}}$
Theoretical foundation	Heuristic	COI	Decoupling ($\Delta \mathbf{V} = \mathbf{0}$)	Decoupling ($\Delta \mathbf{V} \neq \mathbf{0}$)
Suit for zero-inertia system?	No	Yes	Yes	Yes
Could analyze bus weighting?	-	No	Yes	Yes
Could analyze voltage impact?	-	No	No	Yes

* \mathbf{J} is the vector of inertia

2) System Frequency Analysis Models

The ASF is a traditional system frequency analysis model. The basic idea is to approximately calculate COI frequency with dynamics of devices [8]. For an easier derivation, certain assumptions such as constant voltages are made. As a result, the analysis results may lack accuracy, particularly when voltage dynamics cannot be disregarded. Besides, strictly speaking, the ASF model cannot be applied to zero-inertia systems since its derivation relies on the concept of COI. Nevertheless, it can be observed from its transfer function that the ASF can still be computed in such scenarios, albeit as a pragmatic approach that lacks a theoretical foundation.

The CMF and VCMF are obtained by decoupling the frequency responses and thus are more theoretically rigorous. We note that their expressions are consistent if the voltage is constant. In such cases, the VCT is zero and the weighing coefficients of CMF and VCMF are both determined by $L_{\theta p}$. If the network is further lossless (no CILs), their expressions will be the same as ASF, since $c_i = 1$ in this case [12].

In summary, VCMF is more theoretically rigorous than COI frequency and ASF. It can be viewed as the extension of ASF and CMF. The consideration of the VCT allows for the analysis of voltage impact, which makes the VCMF more accurate and comprehensive.

However, the VCT couples the dynamics of all devices, making it generally challenging to obtain an analytic expression. To solve this problem, the next section gives a method to decompose the VCT into several low-order terms, which helps to simplify the analysis and understand the impacts of voltage on the system frequency.

IV. DECOUPLING OF VOLTAGE COUPLING TERM

This section approximately decomposes the VCT into several terms based on the block diagonal property of the network matrix, which simplifies the analysis of VCMF.

A. Decoupling Method of the VCT

For the sake of clarity, the VCT in (15) is rewritten as:

$$\begin{aligned} & \mathbf{c}^T \mathbf{H}_{VP}(s) \mathbf{H}_{VQ}^{-1}(s) \mathbf{H}_{\theta Q}(s) \mathbf{1} \\ &= \underbrace{(\mathbf{c}^T \mathbf{G}_{VP}(s) + \mathbf{c}^T \mathbf{L}_{VP})}_{\text{Row Vector}} \cdot \underbrace{(\mathbf{G}_{VQ}(s) + \mathbf{L}_{VQ})^{-1}}_{\text{Square Matrix}} \cdot \underbrace{\mathbf{G}_{\theta Q}(s) \mathbf{1}}_{\text{Column Vector}} \end{aligned} \quad (16)$$

where $\mathbf{L}_{\theta Q} \mathbf{1} = \mathbf{0}$ is used.

The above equation shows that the VCT is computed by multiplying three parts: a row vector, a square matrix, and a column vector. Note that the i -th element of the row vector/column vector is only related to the i -th device. But the elements in the inverse of the middle square matrix may be relevant to almost all the devices in the system, due to the fact that \mathbf{L}_{VQ} is typically full (passive buses are reduced). Thus, it can be concluded that the inverse of the middle matrix introduces the coupling among all the devices, and the key to simplifying the VCT is to simplify the \mathbf{L}_{VQ} matrix.

As analyzed in Section II-B, the matrix \mathbf{L}_{VQ} is generally block diagonally dominated. If the elements in the off-diagonal block can be ignored, then the VCT is approximately

decomposed into several terms, and each term is only related to the devices in each block, as illustrated in Fig. 2. We note that the simplification of \mathbf{L}_{VQ} can be interpreted as cut off some weak Q-V path in the F-Q-V-P response. It transforms the VCT from globally coupling to locally coupling, which simplifies the analysis of VCT and VCMF.

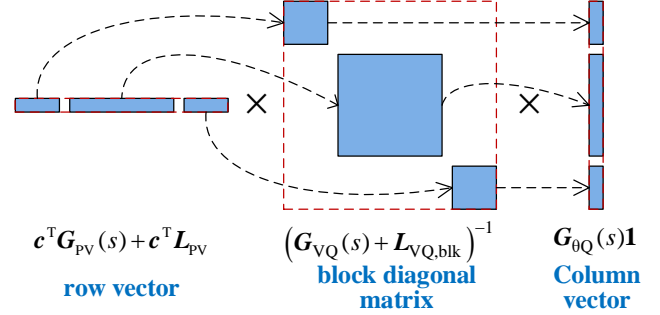


Fig. 2. Schematic diagram of the decoupling of VCT.

Suppose that the power system is already partitioned into m regions (how to partition will be discussed in the next subsection), and denote the simplified \mathbf{L}_{VQ} matrix by $\mathbf{L}_{VQ,blk}$, then the approximate VCMF (xVCMF) can be expressed as:

$$\Delta\omega_{aVCM} = \frac{\mathbf{c}^T \Delta \mathbf{P}_D}{\sum_{i=1}^n c_i G_{\theta P,i}(s) - \sum_{i=1}^m \mathbf{H}_{VP,blk,i} \mathbf{H}_{VQ,blk,i}^{-1} \mathbf{H}_{\theta Q,blk,i}} \frac{s}{\omega_0} \quad (17)$$

where $\mathbf{H}_{VP,blk,i}$ and $\mathbf{H}_{\theta Q,blk,i}$ are respectively the i -th sub-vector of \mathbf{H}_{VP} and $\mathbf{H}_{\theta Q}$; $\mathbf{H}_{VQ,blk,i}$ is the i -th block of $\mathbf{H}_{VQ,blk}$. The “ s ” is omitted for notational simplicity.

B. Partitioning of the Network

Power system partitioning is a widely studied problem, and there are many well-established methods [19],[21]–[22]. For the concern of this paper, the partitioning problem can be described as the following optimization problem

$$\begin{aligned} & \min_{e \in E} \delta \\ & \text{s.t.} \quad \max_i \text{size}(\mathbf{L}_{VQ,blk,i}) \leq N_{\max} \end{aligned} \quad (18)$$

where E denotes the set of all partitioning strategies and e is one of them. The notation $\text{size}(\mathbf{A})$ denotes the number of rows of matrix \mathbf{A} . The constraint ensures the number of devices in each block is not greater than the allowed value N_{\max} , which makes the calculation and analysis of VCMF simple enough. The choice of N_{\max} depends on the desired calculation burden. A larger N_{\max} yields more accurate results but also increases the computational complexity. It should be noted that if the devices are reasonably aggregated firstly (e.g., aggregating a wind farm), the N_{\max} can be significantly reduced while achieving the same accuracy. δ denotes the relative error of the middle matrix in VCT and its simplification, as (19). Minimizing δ ensures the xVCMF is as accurate as possible.

$$\delta = \frac{\left\| (\mathbf{G}_{VQ}(s) + \mathbf{L}_{VQ})^{-1} - (\mathbf{G}_{VQ}(s) + \mathbf{L}_{VQ,blk})^{-1} \right\|}{\left\| (\mathbf{G}_{VQ}(s) + \mathbf{L}_{VQ})^{-1} \right\|} \quad (19)$$

where $\|\mathbf{A}\|$ denotes the matrix norm of \mathbf{A} , such as the \mathcal{H}_∞ norm.

> REPLACE THIS LINE WITH YOUR MANUSCRIPT ID NUMBER (DOUBLE-CLICK HERE TO EDIT) <

The optimization problem (18) is combinatorial and computationally hard, considering the number of possible partitioning strategies is huge. Here we propose a method to obtain the suboptimal solution based on algebraic graph theory.

Given a Laplacian matrix of a graph, the second-smallest eigenvalue, known as the algebraic connectivity, is a measure that provides insights into the connectivity and structure of the graph [23]. Smaller algebraic connectivity indicates a stronger separation between two subgraphs, i.e., with fewer edges (or their weightings are smaller) connecting the two parts. Additionally, the sign of the elements in the corresponding eigenvector can be used to distinguish the two subgraphs [24].

To minimize δ , it is crucial to carefully select the small off-diagonal elements of L_{VQ} (weak Q-V connection in the system) to be neglected. In this regard, a Laplacian matrix can be formulated based on L_{VQ} to identify these weak couplings. Thus, a suboptimal yet effective solution to the optimization problem (18) can be obtained, as follows.

1) Define Laplacian matrix $L_{VQ,L} = \text{triu}(L_{VQ}) + \text{triu}(L_{VQ})^T - \text{diag}(\text{triu}(L_{VQ}) + \text{triu}(L_{VQ})^T)\mathbf{1}$. Note that L_{VQ} exhibits near symmetry, making use of either its upper or lower triangle equivalent. Then partitioning the power system (L_{VQ}) into two regions (two diagonal-block) according to the algebraic connectivity and corresponding eigenvector of $L_{VQ,L}$.

2) For each region, if the number of containing devices exceeds the given N_{\max} , partition the region into two sub-regions similar to step 1.

3) Repeat step 2 iteratively until the number of devices in all regions is not greater than N_{\max} .

The proposed method significantly reduces the computational complexity compared to an exhaustive search, making it applicable to large-scale power systems. Then xVCMF can be calculated and analyzed easily.

V. CASE STUDY

In this section, the validity of VCMF and xVCMF are validated via numerical simulations using MATLAB/Simulink. We note that the simulations are conducted using high-fidelity and nonlinear electromagnetic models, rather than the linearized electromechanical model used in the analysis.

A. Test System Descriptions

Two test systems are utilized in the case study, illustrated in Fig. 3. The power base value for both systems is 600 MVA, and the nominal frequency is 60 Hz. There are three types of generation devices, i.e., SGs, GFL and GFM converters. The GFL converters are equipped with F-P and F-Q droop [13], with gain D_{GFL} and K_{FQ} respectively. The GFM operates as a VSG, with virtual inertia J_{GFM} and damping coefficient D_{GFM} . Detailed models and parameters of these devices can be founded in Appendix-A unless otherwise specified.

The 2-gen system is employed to illustrate the importance of considering voltage dynamics in the analysis of frequency, such as when the converter adopts the F-Q droop control. The system comprises a GFL converter, a GFM converter and a CIL. The parameters of the load and transmission lines are R_L

$= 1$ pu, $X_L = 8$ pu, and $X_1 = X_2 = 0.2$ pu

The 10-gen system is further utilized to demonstrate the applicability of the proposed VCMF, as well as its simplification xVCMF in larger-scale power systems. The test system consists of 5 GFL converters, 3 GFM converters and 2 SGs. To highlight the advantages of VCMF over ASF and CMF, the system includes a large amount of CILs, located at bus 15, 16, 18, 21, 24, 26, 27 and 28 (same as [12]). These loads collectively consume approximately 8 pu active power and 1 pu reactive power. The network parameters are identical to those of the IEEE standard 39-bus system [25].

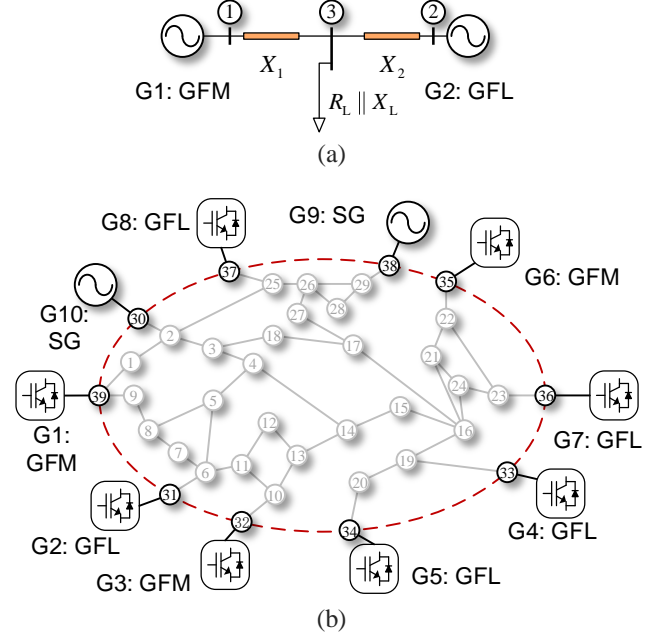


Fig. 3. Schematic diagram of test systems: (a) 2-gen test system, (b) 10-gen test system.

TABLE II.
WEIGHTING VECTORS OF TEST SYSTEMS

Test system	weighting coefficients	
2-gen	$c_1 = 0.983, c_2 = 1.017$	$c_1^{(3)} = 1.000, c_2^{(3)} = 1.036, c_3^{(3)} = 0.964$
	(load as a part of network)	(load as a device)
10-gen	$c_1 = 1.001, c_2 = 1.053, c_3 = 1.059, c_4 = 1.030, c_5 = 1.020,$	
	$c_6 = 0.966, c_7 = 0.965, c_8 = 1.080, c_9 = 0.826, c_{10} = 1.000$	

TABLE II presents the weighting coefficients of the two systems according to (13). In the 2-gen system, two perspectives are compared, i.e., consider the CIL as part of the network or as a device. In the latter case, the system consists of 3 devices.

B. Case Studies on the 2-gen Test System

In the 2-gen system, the virtual inertia of the GFM converter is set to 0, resulting in a zero-inertia system. Thus, the COI frequency cannot be calculated.

Assuming a power step of 0.2 pu occurs in G1, i.e. $\Delta P_{D1}(s) = -0.2/s$, Fig. 4 (a) depicts the bus frequency trajectories for different F-Q droop gain K_{FQ} . As K_{FQ} increases, the frequencies show a significant rise, which can be explained by

> REPLACE THIS LINE WITH YOUR MANUSCRIPT ID NUMBER (DOUBLE-CLICK HERE TO EDIT) <

Fig. 4 (b). When the frequency drops, the negative F-Q droop gain (opposite to the F-P loop) causes the converter to output less reactive power. Consequently, the load voltage and active power consumption decrease, resulting in a reduction in the frequency drop. Therefore, larger negative values of K_{FQ} lead to lower load voltage and higher frequency trajectories.

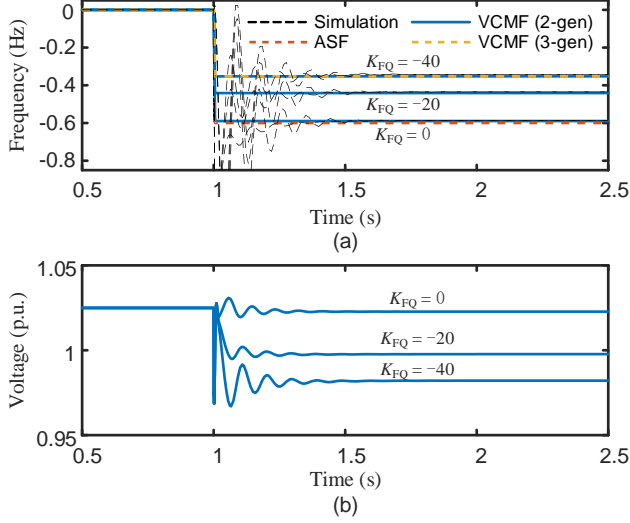


Fig. 4. Time-domain simulation and theoretical results in the 2-gen system. (a) Comparison of the frequency trajectories obtained by simulations, ASF and VCMF. (b) Trajectories of load voltage.

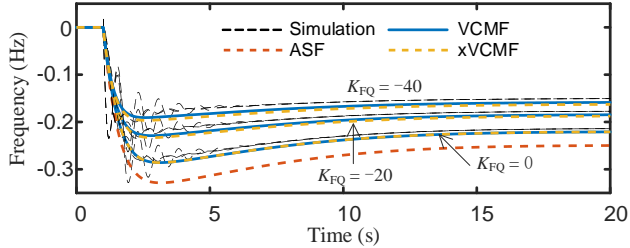


Fig. 5. Frequency trajectories obtained by time-domain simulations and theoretical analyses in the 10-gen system.

TABLE III.

COMPARISON OF QUASI-STEADY-STATE FREQUENCY OBTAINED BY SIMULATIONS AND THEORETICAL ANALYSES

	K_{FQ}/pu	Simu/Hz	ASF/Hz	CMF/Hz	VCMF/Hz
2-gen	0	-0.587	-0.600 (2.3%)	-0.590 (0.5%)	-0.590 (0.5%)
	-20	-0.435	-0.600 (38.0%)	-0.590 (35.6%)	-0.441 (1.5%)
	-40	-0.342	-0.600 (75.3%)	-0.590 (72.2%)	-0.353 (3.0%)
	K_{FQ}/pu	Simu/Hz	ASF/Hz	xVCMF/Hz	VCMF/Hz
10-gen	0	-0.214	-0.250 (16.8%)	-0.221 (3.2%)	-0.221 (3.2%)
	-20	-0.177	-0.250 (24.5%)	-0.187 (5.8%)	-0.184 (4.2%)
	-40	-0.150	-0.250 (66.3%)	-0.162 (8.1%)	-0.158 (5.3%)

According to TABLE I and Appendix-B, the VCMF and ASF in this system can be calculated as follows (the CMF is the same as the VCMF in the case of $K_{FQ} = 0$).

$$\Delta\omega_{VCM}(s) = \frac{c_1 \Delta P_{D1}(s)}{c_1 D_{GFM} + c_2 D_{GFL} - \frac{(c_1 L_{VP,12} + c_2 L_{VP,22}) K_{FQ}}{L_{VQ,22}}} \quad (20)$$

$$= \frac{c_1 \Delta P_{D1}(s)}{c_1 D_{GFM} + c_2 D_{GFL} - 0.336 K_{FQ}}$$

$$\Delta\omega_{AS}(s) = \frac{\Delta P_{D1}(s)}{D_{GFM} + D_{GFL}} \quad (21)$$

It can be inferred from (20) that the F-Q droop has a similar effect to the F-P droop. Its effect is influenced by network structure, parameters (including reduced load) and the value of K_{FQ} . When $K_{FQ} = -20$ pu or -40 pu, the equivalent frequency damping is respectively 6.72 pu and 13.44 pu, which is comparable to the damping provided by converters, i.e., $D_{GFM} + D_{GFL} = 20$ pu.

Fig. 4 (a) shows the VCMF and ASF in (20) and (21). And the error analysis is provided in TABLE III, where the simulation results serve as the reference. Notably, the relative errors of the ASF and CMF can reach up to 70%, whereas that of VCMF remains below 5%. These results emphasize the importance of considering voltage dynamics and demonstrate the efficacy of VCMF in accurately characterizing the system frequency response.

The VCMF can also be calculated if the CIL is viewed as a device, as in (22), where the superscript (3) denotes 3-gen. It can be clearly observed that the equivalent damping is mainly the result of the combination of F-Q droop and CIL load. If the numerator and denominator in (20) and (22) are divided by c_1 or $c_1^{(3)}$ at the same time, respectively, the two expressions of VCMF are exactly the same. It is also verified in Fig. 4 (a), taking the case of $K_{FQ} = -40$ pu as an example.

$$\Delta\omega_{VCM}^{(3)}(s) = \frac{c_1^{(3)} \Delta P_{D1}(s)}{c_1^{(3)} D_{GFM} + c_2^{(3)} D_{GFL} - (0.021 + 0.321 R_L^{-1}) K_{FQ}} \quad (22)$$

$$= \frac{c_1^{(3)} \Delta P_{D1}(s)}{c_1^{(3)} D_{GFM} + c_2^{(3)} D_{GFL} - 0.342 K_{FQ}}$$

Because considering the loads as parts of the network can significantly reduce the number of devices, we will adopt this perspective in the next test system.

C. Case Studies on the 10-gen Test System

Considering a power step disturbance of 0.5 pu occurring in G9 of the 10-gen system, Fig. 5 presents the bus frequency trajectories obtained by simulations and theoretical analysis. The corresponding relative errors are also provided in TABLE III. It can be observed that as the system scale and complexity increase, the errors of VCMF slightly increase compared to the previous test system, but it remains significantly more accurate than ASF. Notably, even when $K_{FQ} = 0$, ASF differs considerably from the simulation results, due to the assumption of equal weightings for each bus. However, c_9 is only 0.826, indicating that the impact of the disturbance located at G9 is 17.4% less significant than suggested by ASF.

In the following, the effectiveness of the network partitioning and xVCMF will be verified. Firstly, the network partitioning method proposed in Section IV-B is applied. Fig.

6 gives the partitioning results and the relative error δ (calculated by (19)), for different N_{\max} . Each pair of split lines in Fig. 6 (a) correspond to a step of δ in Fig. 6 (b). For instance, when N_{\max} is set to 10, there is no need for partitioning, and the δ is zero. When $N_{\max} = 6, 7, 8$, or 9 , the network will be divided into two regions, i.e., $\{G1-G3, G8-G10\}$ and $\{G4-G7\}$, and δ rises to 2.3%.

It can be observed from Fig. 6 (a) that most off-diagonal elements in L_{VQ} matrix is very small, which allows the proposed partitioning method to effectively separate the power network while preserving main couplings. Even when N_{\max} is set to 2, the relative error δ is only 5.0%. Thus, we choose $N_{\max} = 2$ to calculate the xVCMF. It is compared to VCMF in Fig. 5 (a) and TABLE III. The results illustrate that xVCMF closely approximates VCMF and is significantly more accurate than ASF, even in the case of $K_{FQ} = 40$ pu.

For a comprehensive analysis, TABLE IV shows the equivalent frequency damping provided by F-Q droop in each partitioning region, considering the case of $K_{FQ} = -40$ pu. It can be observed that although all GFL converters share the same K_{FQ} , the damping values of each converter (or region) vary significantly. This discrepancy is closely related to the distribution of converters and loads within the system. Additionally, the sum of damping across all regions is found to be monotonically non-decreasing as N_{\max} increases. Notably, when N_{\max} is set to 2, the sum of damping is very close to that obtained when N_{\max} is set to 10. This further validates the effectiveness of the network partitioning method the xVCMF.

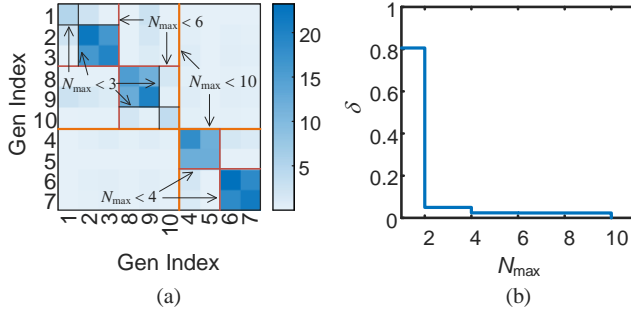


Fig. 6. The partitioning results for different N_{\max} . (a) The heatmap of L_{VQ} matrix with split lines, where the order of devices is readjusted. (b) relative error δ .

TABLE IV
EQUIVALENT FREQUENCY DAMPING OF EACH REGION
PROVIDED BY F-Q DROOP (PU VALUES)

N_{\max}	G1	G2	G3	G8	G10	G9	G4	G5	G6	G7	Sum
1	0	1.67	0	2.74	0	0	17.43	1.01	0	2.80	25.64
2	0	1.67		2.74		0	36.12		2.80		43.32
3		1.67			2.74		36.12		2.80		43.32
4-5		1.67			2.74			41.02			45.42
6-9				4.45				41.02			45.47
10											47.08

In conclusion, the proposed VCMF is suitable for representing system frequency even in the scenario of zero-inertia, where COI frequency cannot be calculated. Besides,

the VCMF proves to be highly effective in accurately characterizing the frequency responses of power systems, even with large variations of bus voltages. In contrast, traditional methods like ASF and earlier CMF exhibit notable deviations from the system frequency when voltage dynamics play a significant role. Additionally, the partitioning of the network in large-scale power systems can be achieved by selectively ignoring certain non-diagonal elements of the L_{VQ} matrix, based on the algebraic connectivity of the constructed Laplacian matrix. This partitioning approach greatly facilitates the calculation and analysis of VCMF, making it suitable for practical applications in large-scale power systems.

VI. CONCLUSIONS

This paper defined a VCMF to understand and analyze the frequency response of power systems, particularly in the cases where the dynamics of bus voltages cannot be ignored. It has been demonstrated that:

1) The VCMF offers an improved understanding of the system frequency compared to the traditional COI frequency. It demonstrates that the system frequency may not be merely an inertia-weighted average but rather a common component of the bus frequencies. This common part of the bus frequencies stems from the rotational invariance of power flow. This new perspective allows for analyzing the system-level frequency even in zero-inertia systems.

2) By incorporating the indirect F-P responses caused by voltage dynamics, VCMF provides a more precise and comprehensive characterization of the system's frequency behaviors compared to ASF and CMF. This is demonstrated through test systems where converters are equipped with the F-Q droop. It is revealed that the F-Q droop exhibits similar effects to the F-P droop (i.e. frequency damping) when CILs are present nearby. The electromagnetic simulations indicate that VCMF significantly reduces the error in determining the frequency response in this situation (reducing the error from up to 60%-70% to approximately 5%).

3) Analyzing VCMF in large-scale power systems can be challenging due to the complexity and computational burden associated with the globally coupling term. To address this, a network partitioning method is proposed based on the algebraic connectivity of the constructed $L_{VQ,L}$ matrix. This method selectively neglects the small non-diagonal elements in the L_{VQ} matrix, effectively cutting the weak path in the Q-V responses. Then the globally coupling term is decomposed into several locally coupling terms. The resulting xVCMF exhibits similar behaviors to the original VCMF.

The analysis of VCMF is under the assumption of linearization, which may be necessary considering the complexity of large-scale nonlinear systems. There are some practical methods for addressing the nonlinearity, as discussed in [12]. For example, replace the transfer functions $G_{OP,i}(s)$ with nonlinear models that incorporate factors such as dead-zones, in the calculation of VCMF. We note that it is possible to rigorously extend VCMF to the nonlinear case, considering that the foundation of VCMF, namely the rotational invariance

> REPLACE THIS LINE WITH YOUR MANUSCRIPT ID NUMBER (DOUBLE-CLICK HERE TO EDIT) <

of power flow, still holds in the nonlinear case. We consider this as a future direction.

REFERENCES

- [1] F. Milano, F. Dörfler, G. Hug, D. J. Hill, and G. Verbić, "Foundations and challenges of low-inertia systems," in *Proc. 20th Power Syst. Comput. Conf.*, Dublin, Ireland, pp. 1–25, 2018.
- [2] National grid ESO, "Technical Report on the events of 9 August 2019," N.G., Warwick, UK, Tech. Rep., 2019.
- [3] B. Magness, "Review of Feb. 2021 Extreme Cold Weather Event-Ercot Presentation," ERCOT, Texas, US, Tech. Rep., 2021.
- [4] N. Hatziaargyriou, J. Milanovic, C. Rahmann, V. Ajjarapu, C. Canizares, I. Erlich, D. Hill, et al. "Definition and classification of power system stability—revisited & extended," *IEEE Trans. Power Syst.*, vol. 36, no. 4, pp. 3271–3281, Jul. 2021.
- [5] P. Kundur et al., "Definition and classification of power system stability IEEE/CIGRE joint task force on stability terms and definitions," *IEEE Trans. Power Syst.*, vol. 19, no. 2, pp. 1387–1401, May 2004.
- [6] M. Wang, J. Guo, S. Ma, T. Wang, X. Zhang, K. Luo, and G. Wang, "Review of Transient Frequency Stability Analysis and Frequency Regulation Control Methods for Renewable Power Systems," *Proc. CSEE*, vol. 43, no. 05, pp. 1672–1694, 2023.
- [7] Z. Lu, Y. Ye, L. Guo et al., "Frequency regulation challenge of power electronics dominated power systems and its new multi-level coordinated control framework," *Electr. Power*, vol. 52, no. 4, pp. 8–17, Aug. 2019.
- [8] M. L. Chan, R. D. Dunlop, and F. Schweppe, "Dynamic equivalents for average system frequency behavior following major disturbances," *IEEE Trans. Power Appar. Syst.*, vol. PAS-91, no. 4, pp. 1637–1642, Jul. 1972.
- [9] P. M. Anderson and M. Mirheydar, "A low-order system frequency response model," *IEEE Trans. Power Syst.*, vol. 5, no. 3, pp. 720–729, Aug. 1990.
- [10] D. Obradovic, M. Dijokas, G. Misyris, T. Weckesser, and T. Van Cutsem, "Frequency dynamics of the Northern European AC/DC power system: a look-ahead study," *IEEE Trans. Power Syst.*, vol. 37, no. 6, pp. 4661–4672, 2022.
- [11] Z. Li, X. Wu, K. Zhuang, L. Wang, Y. Miao, and B. Li, "Analysis and reflection on frequency characteristics of East China Grid after bipolar locking of 9.19 Jinping-Sunan DC transmission line," *Autom. Elect. Power Syst.*, vol. 41, no. 7, pp. 149–155, May 2017.
- [12] H. Gao, H. Xin, L. Huang, Z. Li, W. Huang, C. Wu, and P. Ju, "Common-Mode Frequency in Inverter-Penetrated Power Systems: Definition, Analysis, and Quantitative Evaluation," *IEEE Trans. Power Syst.*, vol. 37, no. 6, pp. 4846–4860, Nov. 2022.
- [13] W. Zhong, G. Tzounas, and F. Milano, "Improving the power system dynamic response through a combined voltage-frequency control of distributed energy resources," *IEEE Trans. Power Syst.*, vol. 37, no. 6, pp. 4375–4384, 2022.
- [14] F. Paganini and E. Mallada, "Global Analysis of Synchronization Performance for Power Systems: Bridging the Theory-Practice Gap," *IEEE Trans. Autom. Control*, vol. 65, no. 7, pp. 3007–3022, July 2020.
- [15] C. Yang, L. Huang, H. Xin, and P. Ju, "Placing grid-forming converters to enhance small signal stability of PLL-integrated power systems," *IEEE Trans. Power Syst.*, vol. 36, no. 4, pp. 3563–3573, Jul. 2020.
- [16] F. Milano and Á. Ortega, "Frequency divider," *IEEE Trans. Power Syst.*, vol. 32, no. 2, pp. 1493–1501, Mar. 2017.
- [17] Y. Chen, K. Lao, D. Qi, H. Hui, S. Yang, Y. Yan, and Yi Zheng, "Distributed Self-triggered Control for Frequency Restoration and Active Power Sharing in Islanded Microgrids," *IEEE Trans. Industr. Inform.*, early access, doi: 10.1109/TII.2023.3240738.
- [18] F. Dörfler and F. Bullo, "Synchronization in complex networks of phase oscillators: A survey," *Automatica*, vol. 50, no. 6, pp. 1539–1564, Jun. 2014.
- [19] W. Hao, Z. Huang, J. Lu, Y. Zhou, S. Liao, W. Wang, M. Chen, and D. Gan, "Structural Properties of V-Q Jacobian Matrix and Voltage Stability Analysis of Power Network With Photovoltaic Penetration," *Proc. CSEE*, vol. 43, no. 05, pp. 1719–1730, 2023.
- [20] G. W. Stewart, and J. Sun. *Matrix perturbation theory*. New York: Academic press, 1990.
- [21] A. Sen, P. Ghosh, V. Vittal, and B. Yang, "A new min-cut problem with application to electric power network partitioning," *Eur. Trans. Electr. Power*, vol. 19, no. 6, pp. 778–797, Sep. 2009.
- [22] L. Sun et al., "Network partitioning strategy for parallel power system restoration," *IET Gener. Transm. Distrib.*, vol. 10, no. 8, pp. 1883–1892, 2016.
- [23] F. Dörfler, J. W. Simpson-Porco, and F. Bullo, "Electrical networks and algebraic graph theory: Models, properties, and applications," *Proc. IEEE*, vol. 106, no. 5, pp. 977–1005, May 2018.
- [24] F. Bullo, *Lectures on Network Systems*. Seattle, WA, USA: Kindle Direct Publishing, 2019.
- [25] I. Hiskens, "39-bus system (New England Reduced Model)," *IEEE PES Task Force on Benchmark Systems for Stability Controls*, Tech. Rep., Nov. 2013.
- [26] P. Kundur, *Power System Stability and Control*. New York, NY, USA: McGraw-Hill, 1994.
- [27] B. K. Poolla, D. Groß, and F. Dörfler, "Placement and implementation of grid-forming and grid-following virtual inertia and fast frequency response," *IEEE Trans. Power Syst.*, vol. 34, no. 4, pp. 3035–3046, 2019.

APPENDIX

A. Detailed Models of Generation Devices

Models of the SG, GFL and GFM converter used in simulations are shown in Fig. 7. In Fig. 7 (a), the equation of winding, AVR and power calculation are as follows:

$$\begin{cases} T_d' \dot{E}_q' = -\frac{x_d - x_d'}{x_d' - x_d'} E_q' + \frac{x_d - x_d'}{x_d' - x_d'} E_q'' + E_{fd} \\ T_d'' \dot{E}_q'' = E_q' - E_q'' - (X_d' - X_d'') i_d \\ T_q' \dot{E}_d' = -\frac{x_q - x_q'}{x_q' - x_q'} E_d' + \frac{x_d - x_q'}{x_q' - x_q'} E_d'' \\ T_q'' \dot{E}_d'' = E_d' - E_d'' - (X_q' - X_q'') i_d \\ V_d = E_d'' + X_q'' i_q \\ V_q = E_q'' - X_d'' i_d \end{cases} \quad (23)$$

$$\begin{cases} E_{fd} = \frac{K_V}{T_V s + 1} (V_{ref} - V_{abs}) \\ V_{abs} = \sqrt{V_d^2 + V_q^2} \end{cases}, \quad \begin{cases} P = E_d'' I_d + E_q'' I_q \\ Q = -E_d'' I_q + E_q'' I_d \end{cases} \quad (24)$$

where T_d' (T_q') and T_d'' (T_q'') are the d-axis (q-axis) transient and subtransient time constants, V_d (V_q), E_d' (E_q') and E_d'' (E_q'') are the d-axis (q-axis) stator voltages, transient and subtransient internal voltages, X_d (X_q), X_d' (X_q') and X_d'' (X_q'') are the d-axis (q-axis) reactance, transient and subtransient reactances, E_{fd} is the excitation voltage, K_V and T_V are respectively the gain and time constant of AVR, V_{abs} and V_{ref} are amplitude and reference values of the terminal voltage, K_{SG} is the gain of PFR, K_1 , K_3 , K_5 and K_7 are the gains of the turbine governor, and $T_1 - T_7$ are its time constants.

For the GFL converter (Fig. 7 (b)), the dynamics of the LC filter can be formulated as

$$\begin{cases} \mathbf{E}_{xy} - \mathbf{V}_{xy} = (R_F + sL_F + j\omega_0 L_F) \mathbf{I}_{xy} \\ \mathbf{I}_{xy} - \mathbf{I}_{oxy} = (sC_F + j\omega_0 C_F) \mathbf{V}_{xy} \end{cases} \quad (25)$$

where L_F , C_F and R_F are respectively the inductance resistance and capacitance of LC filter, $\mathbf{E}_{xy} = E_x + jE_y$ and $\mathbf{V}_{xy} = V_x + jV_y$ are the converter modulation voltage and capacitor voltage, $\mathbf{I}_{xy} = I_x + jI_y$ and $\mathbf{I}_{oxy} = I_{ox} + jI_{oy}$ are the inductor current and the current injected into the AC network.

The active/reactive power are calculated similarly to (24). The dynamic equations of the current control, power control,

> REPLACE THIS LINE WITH YOUR MANUSCRIPT ID NUMBER (DOUBLE-CLICK HERE TO EDIT) <

PLL, the F-P droop and F-Q droop control [13] are as follows:

$$\mathbf{E}_{dq} = G_{CC}(s)(\mathbf{I}_{dq}^{\text{ref}} - \mathbf{I}_{dq}) + j\omega_0 L_F \mathbf{I}_{dq} + f_{VF}(s) \mathbf{V}_{dq} \quad (26)$$

$$\begin{cases} I_d^{\text{ref}} = G_{PC}(s)(P^{\text{ref}} - P) \\ I_q^{\text{ref}} = G_{PC}(s)(Q - Q^{\text{ref}}) \end{cases} \quad (27)$$

$$\begin{cases} \dot{\theta}_{\text{PLL}} = \omega_0 \omega_{\text{PLL}} \\ T_{L,F} \dot{\omega}_{\text{PLL}} = -\omega_{\text{PLL}} + K_{L,P} V_q + K_{L,I} \int V_q \end{cases} \quad (28)$$

$$\begin{cases} P^{\text{ref}} = P_0 - D_{\text{GFL}}(\omega_{\text{PLL}} - 1) \\ Q^{\text{ref}} = Q_0 - K_{\text{FQ}}(\omega_{\text{PLL}} - 1) \end{cases} \quad (29)$$

where $G_{CC}(s) = K_{CC,P} + K_{CC,I}/s$ is the PI regulator of current control loop, $f_{VF}(s) = K_{VF}/(sT_{VF} + 1)$ is the filter of the voltage feedforward control, $G_{PC}(s) = K_{PC,P} + K_{PC,I}/s$ is the PI regulator of power control loop, $T_{L,F}$ is the time constant of PLL, and $K_{L,P}$ and $K_{L,I}$ are respectively the proportion and integral coefficients of PLL, D_{GFL} and K_{FQ} are respectively the F-P and F-Q droop coefficients.

In Fig. 7 (c), the dynamics of the LC, current control and the calculation of power are the same as those in the GFL converter, the dynamics of voltage control is

$$\mathbf{I}_{dq}^{\text{ref}} = G_{VC}(s)(\mathbf{V}_{dq}^{\text{ref}} - \mathbf{V}_{dq}) + j\omega_0 C_F \mathbf{V}_{dq} + k_{IF} \mathbf{I}_{odq} \quad (30)$$

where $G_{VC}(s) = K_{VC,P} + K_{VC,I}/s$ is the PI regulator of voltage control loop, k_{IF} is the current feedforward coefficient.

The main parameters of these three types of generation devices are given in TABLE V, due to page limits, we do not give all parameters, they can be referred to [15],[25]-[27].

TABLE V
MAIN PARAMETERS OF GENERATION DEVICES

$J_{SG} = 10$	$D_{SG} = 0$	$K_{SG} = 20$	$K_1 = 0.22$	$K_3 = 0.22$
$K_5 = 0.3$	$K_7 = 0.26$	$T_1 = 0.2$	$T_2 = 0$	$T_3 = 0.1$
$T_4 = 0.25$	$T_5 = 4$	$T_6 = 4$	$T_7 = 0.4$	$D_{\text{GFL}} = 10$
$J_{\text{GFM}} = 10$	$D_{\text{GFM}} = 10$			

B. Simplified Jacobine Transfer Function Matrixes

The accurate Jacobian matrices based on above models are typical of a high order, which poses challenges in the calculation of VCMF. For instance, it is difficult to precisely obtain the expression of the inverse of $(\mathbf{G}_{VQ}(s) + \mathbf{L}_{VQ})$. Thus, simplified Jacobian matrices are employed in theoretical analysis, as follows:

$$\begin{aligned} (\text{SG}) \quad & \begin{bmatrix} s\omega_0^{-1}(J_{SG}s + D_{SG} + G_T(s)) & 0 \\ 0 & \eta \end{bmatrix} \\ (\text{GFL}) \quad & \begin{bmatrix} s\omega_0^{-1}D_{\text{GFL}} & 0 \\ s\omega_0^{-1}K_{\text{FP}} & 0 \end{bmatrix} \\ (\text{GFM}) \quad & \begin{bmatrix} s\omega_0^{-1}(J_{\text{GFM}}s + D_{\text{GFM}}) & 0 \\ 0 & \eta \end{bmatrix} \end{aligned} \quad (31)$$

where $G_T(s)$ is the transfer function of turbine and governor, as shown in Fig. 7 (a); η is a large number, such as 1×10^6 .

The above simplification is justified by the following reasons: for SGs and GFMs, they can maintain nearly constant voltages, thus they can be approximately modeled as having a

high gain in the V-Q loop, as discussed in Section II-B. For GFL and GFM converters, their power regulation dynamics are typically fast. In this case, the F-P and F-Q loops can be accurately characterized by parameters such as D_{FL} and K_{FP} .

We note that these simplifications may not suit all devices, e.g., where control delays cannot be ignored. However, the primary focus of this paper is to address the recognition and calculation of system frequency in the scenario of non-constant voltages, and these models are considered sufficient to demonstrate the effectiveness of the proposed VCMF. Dealing with more complex models and achieving more accurate calculations using high-order Jacobian matrices will be the subject of future research.

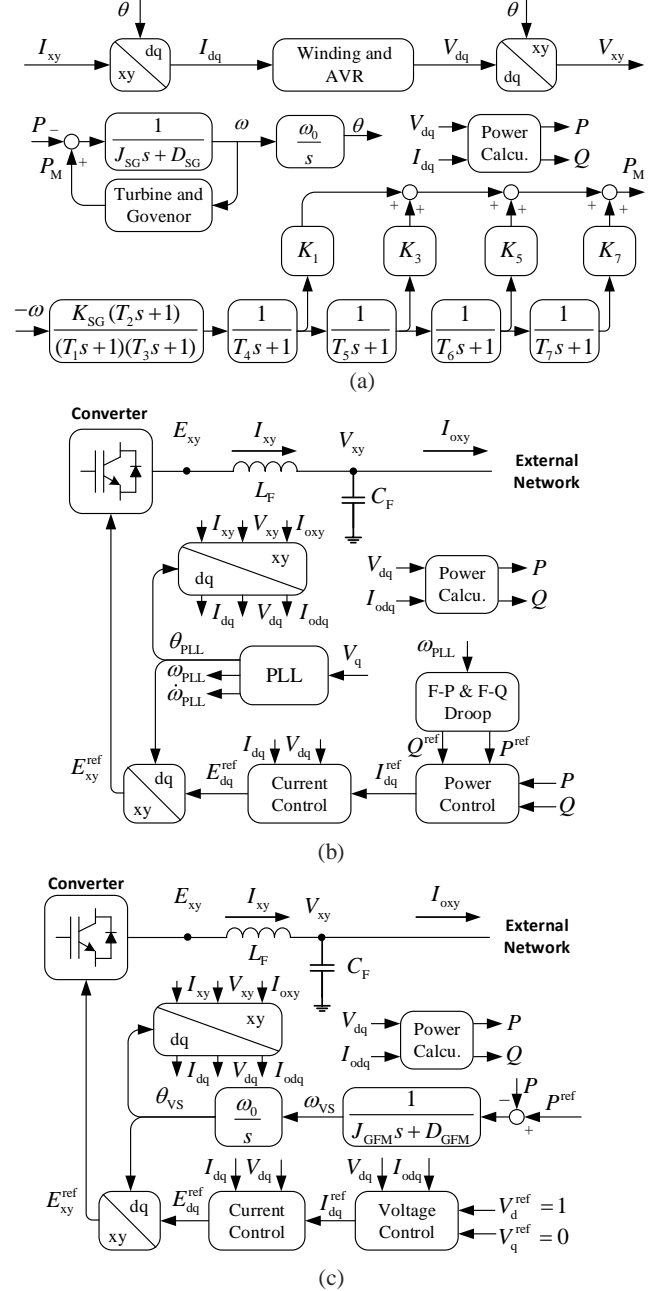


Fig. 7. Models of (a) SG, (b) GFL converter and (c) GFM converter.